Current Chemistry Letters 15 (2026) 117–132

Contents lists available at GrowingScience

Current Chemistry Letters

homepage: www.GrowingScience.com

Optimization of donor units in push–pull thieno[3,2-b]thiophene-based organic dyes: A dft/td-dft study of nineteen candidates for enhanced photovoltaic performance

Mohamed Reda Chriyaa[a], Hayat EL Ouafy[a], Mouna Aamor[a], Walid Iken[a], Loubna Halil[a], Soukaina Naciri[a], Mouad Boutkbout Nait Moudou[a] and Tarik EL Ouafy[b*]

[a]*Laboratory of Engineering in Chemistry and Physics of Matter, Faculty of Sciences and Technics, Sultan Moulay Slimane University, Beni Mellal, Morocco*
[b]*Laboratory of Engineering in Chemistry and Physics of Matter, Faculty of Medicine and Pharmacy, Sultan Moulay Slimane University, Beni Mellal, Morocco*

C H R O N I C L E

Article history:
Received April 12, 2025
Received in revised form
June 14, 2025
Accepted October 8, 2025
Available online
October 8, 2025

Keywords:
DSSCs
Donor Moeities
DFT and TD-DFT
Dye-sensitized solar cells
Thieno[3,2-b]thiophene

A B S T R A C T

Designing high-efficiency sensitizers remains a central challenge for dye-sensitized solar cells (DSSCs). In this work, nineteen donor motifs commonly employed in the literature were screened to identify optimal donors and to assess the impact of donor substitution on the reference dye D_0 (2-cyano-3-[2′-(2″-(4″-(dimethylamino)phenyl)ethynyl)thieno[3,2-b]thiophen-5′-yl]acrylic acid) with the goal of improving device performance. Using DFT/TD-DFT with the CAM-B3LYP functional, we characterized nineteen literature-derived donor motifs via their electronic absorption spectra and key photovoltaic descriptors. Donor substitution, most notably with D_1, D_3, D_5, D_6, and D_{15}, substantially improves the electronic and optical properties, yielding lower HOMO energies, a reduced band gap (E_{gap}), enhanced absorption intensity, and a bathochromic shift of the main band. Performance indicators, notably the electron-injection free energy (ΔG_{inj}) and open-circuit voltage (V_{oc}), indicate spontaneous, thermodynamically favorable electron injection from the excited dye into the TiO_2 conduction band.

1. Introduction

Since the Industrial Revolution, human development-economic, technological, and social, has relied heavily on the exploitation of fossil fuels such as coal, oil, and natural gas. While this intensive use has contributed to significant improvements in living standards, it has also led to serious environmental and social consequences, including global warming, air pollution, the depletion of non-renewable resources, and increased global energy insecurity.[1]

In response to these challenges, a transition toward renewable energy sources, cleaner and more sustainable, has become imperative. Among the various alternatives, solar energy stands out due to its abundant availability, cost-free nature, and lack of pollutant emissions, making it a highly attractive candidate to meet future energy demands. The direct conversion of solar radiation into electricity through photovoltaic technologies is considered one of the most promising approaches for harnessing this resource.[2,3]

In this context, dye-sensitized solar cells (DSSCs), first introduced in 1991 by O'Regan and Grätzel, have attracted growing attention in both fundamental research and industrial applications. These systems are characterized by a relatively simple and modular structure, consisting of a transparent conductive substrate, a nanostructured semiconductor (typically TiO_2), a photosensitizing dye adsorbed onto the surface, a redox electrolyte (commonly based on the iodide/triiodide couple), and a counter-electrode responsible for dye regeneration. The dye plays a crucial role by absorbing light and injecting electrons into the semiconductor, thereby having a direct impact on the overall efficiency of the cell.[4,5]

* Corresponding author
E-mail address tarikelouafy@gmail.com (T. EL Ouafy)

doi: 10.5267/j.ccl.2025.10.005

Currently, DSSCs primarily utilize three main classes of sensitizers: polypyridyl-based ruthenium (II) complexes, porphyrin-derived dyes, and metal-free organic sensitizers. Ruthenium-based dyes have achieved certified power conversion efficiencies of up to 11.6%, while zinc porphyrin co-sensitized DSSCs have recently set a new benchmark, reaching an efficiency of 14.0%.[6,7] However, these first two classes of dyes face significant limitations. Ruthenium (II)-based sensitizers are hindered by the scarcity of the metal, high production costs, and considerable environmental toxicity. Zinc porphyrin dyes, on the other hand, suffer from low synthetic yields and require the use of highly toxic reagents.[8,9] These drawbacks have driven research toward metal-free organic sensitizers, which are increasingly favored due to their widespread availability, low cost, rich structural diversity, vivid coloration, and the high degree of tunability enabled by molecular design.

These sensitizers are typically designed around a donor-π-acceptor (D-π-A) molecular framework, which promotes intramolecular charge transfer and enhances the separation of photoinduced charges. Several structural variations of this motif have been proposed, including D-A-π-A, D-π-A-A, and D-D-π-A configurations, allowing for fine-tuning of the dye's electronic and optical properties.[1,9]

In this context, a recent study conducted by Sen and colleagues emphasized the critical role of structural modifications in enhancing DSSC performance, particularly through the variation of donor groups, π-conjugated linkers, and acceptor units. Their findings demonstrated that incorporating additional spacers within the molecular framework significantly improves sensitizer efficiency. This reinforces the notion that the overall performance of DSSCs is highly dependent on meticulous molecular engineering of the photoactive dye.[10]

In this context, the present study builds upon the work of Fernandes and colleagues,[11] who developed a reference dye (2-Cyano-3-[2′-(2″-(4″-(dimethylamino)phenyl)ethynyl)thieno[3,2-b]thiophen-5′-yl]acrylic acid), denoted here as D_0, featuring a push–pull structure centered on a bithiophene core. This sensitizer achieved a reported power conversion efficiency of approximately 3%, providing a structural foundation for further molecular optimization.[11]

The reference dye D_0 was selected as the model system, having been synthesized and experimentally characterized by Fernandes et al.[11] and exhibiting efficient electronic communication between donor and acceptor fragments (λ_max = 421 nm, $\varepsilon = 3.4 \times 10^4\ M^{-1}\ cm^{-1}$, $\eta = 2.63\%$).[11]

This compound features a well-defined D–π–A architecture that combines an N,N-dimethylaniline donor, an ethynyl–thieno[3,2-b]thiophene π-bridge, and a cyanoacrylic acid acceptor, thereby ensuring extended conjugation and strong electronic communication between fragments. Its near-planar geometry promotes efficient intramolecular charge transfer (ICT) and enables spontaneous electron injection into the TiO_2 conduction band, confirming its suitability as a reference model.[11]

The availability of experimental data for D_0 from the literature further supports validation of the DFT/TD-DFT protocol employed here. By comparing calculated properties (energy levels, absorption spectra, and charge-density distributions)[11] with those measured by Fernandes et al., [11] we confirm the internal consistency of the theoretical methodology. Consequently, dye D_0 provides a robust starting point for the comparative analysis of D_1–D_{19}, enabling a clear assessment of how different donor units influence overall optoelectronic properties and potential DSSC performance.

In addition, several recent studies, were incorporated to update the discussion on modern donor-engineering strategies aimed at improving DSSC performance.[9]

Numerous research efforts, including those from our own group, have focused on introducing targeted structural modifications to this reference molecule. These studies primarily aim to optimize the donor and acceptor units to enhance the photovoltaic performance of dye-sensitized solar cells (DSSCs).[12–15]

In this framework, the present study offers a comparative analysis of 19 dyes derived from the reference D_0 structure, incorporating nineteen distinct donor groups, while keeping the π-conjugated linker and acceptor unit unchanged. Following geometry optimization at the B3LYP/6-311G(d,p), level, the optoelectronic properties of these dyes were evaluated using time-dependent density functional theory (TD-DFT) calculations at the CAM-B3LYP16-311G level.

Fig. 1 displays the donor units, the π-conjugated bridge, and the acceptor group of the reference dye D_0, along with the various substituents introduced on the donor moieties examined in this study. The selection of these donor groups is primarily based on previously reported studies, where they have been recognized as effective and widely employed in D-π-A dye architectures.[15–18]

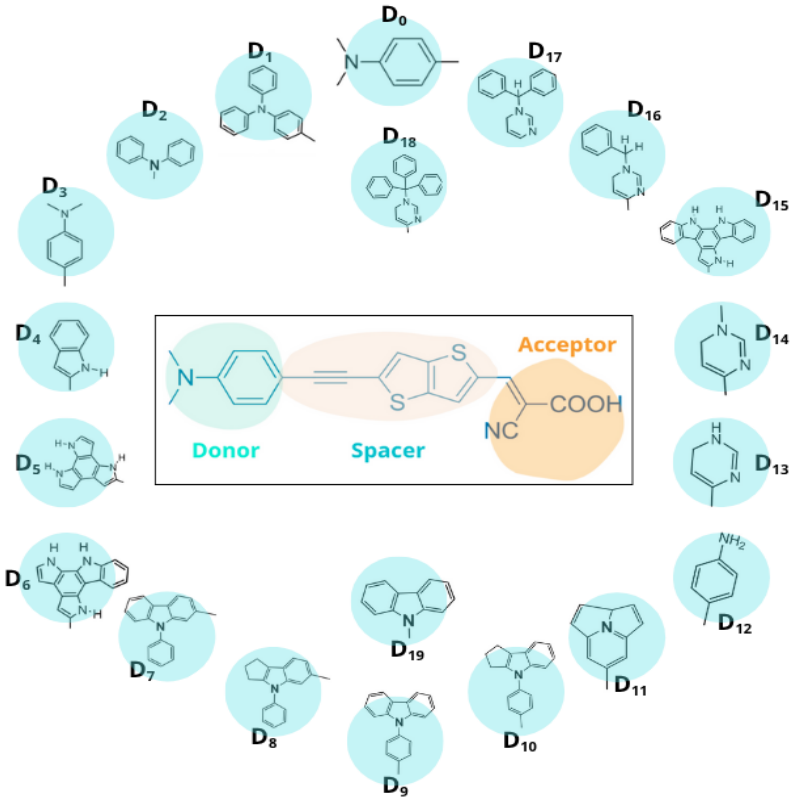

Fig.1. Chemical structure of studied dyes (D_0–D_{19}).

2. Theoretical background and computational methods

2.1. Theoretical background

A wide range of computational parameters can modulate the performance of dye-sensitized solar cells (DSSCs), most notably the power conversion efficiency (η). This efficiency is governed by several device metrics, including the short-circuit current density (J_{SC}), the open-circuit voltage (V_{OC}), the incident solar power (P_{inc}), and the fill factor (FF).[19,20]

$$\eta = \frac{\mathrm{Voc}\,.\,\mathrm{Jsc}\,.\,\mathrm{FF}}{\mathrm{Pinc}}$$

The V_{oc} parameter can be determined using the following analytical relationship:

$$V_{oc} = E_{LUMO} - E_{CB}$$

where E_{LUMO} represents the energy level of the dye, and E_{CB} corresponds to the conduction band energy of TiO_2 (E_{CB} = −4,0 eV).[21] The short-circuit current density (Jsc) represents the number of photons effectively converted into electrical current. It results from a combination of interdependent factors, namely the light-harvesting efficiency (LHE) at a given wavelength (λ), the electron injection efficiency ($\varphi_{(inject)}$), which is directly related to the electron injection driving force ($\Delta G_{(inject)}$), and the charge collection efficiency ($\eta_{(collect)}$). Notably, LHE is governed by the oscillator strength of the dye at its maximum absorption wavelength ($\lambda_{(max)}$).[21,22]

It is crucial to note that the LHE of DSSCs is a key factor affecting their performance. Generally, a high LHE results in a greater amount of photocurrent. The LHE can be calculated using the following equation:[23]

$$LHE = 1 - 10^{-f}$$

where *f* represents the oscillator strength relative to the λ_{max} of the dye. This strength directly influences the LHE. The electron injection driving force ($\Delta G_{(inject)}$) is determined by the energy difference between the dye's excited-state oxidation potential and the conduction band edge of the semiconductor. A more negative $\Delta G_{(inject)}$ value indicates a stronger thermodynamic driving force for electron transfer into the semiconductor. Likewise, the regeneration free energy ($\Delta G_{(regen)}$) of the oxidized dye is evaluated by comparing its ground-state oxidation potential with that of the I^-/I_3^- redox couple.[24]

$$\Delta G_{inject} = E^{dye*} - E_{CB}$$

In this context, E^{dye*} denotes the oxidation potential of the dye in its excited state, while E_{CB} denotes the reduction potential of the conduction band (TiO_2 = − 4.0 eV).[9] The value of E^{dye*} can be determined using the following equation:

$$E^{dye*} = E^{dye} - E^{00}$$

E^{dye} represents the oxidation potential of the molecule in its neutral state ($E^{dye} = -E_{HOMO}$), and E^{00} corresponds to the vertical transition energy to λ_{max}.

To ensure swift electron transfer, ΔG_{reg} needs to be minimized. The driving force for the regeneration of the dye, noted as ΔG_{reg}, is calculated as follows:

$$\Delta G_{reg} = E^{dye} - E_{Redox}^{Electrolyte}$$

where $E_{Redox}^{Electrolyte}$ is the redox potential of the I^-/I^{3-} electrolyte (−4.80 eV).[25]

Using the energy levels of the frontier molecular orbitals (HOMO and LUMO), the chemical potential (μ), electronegativity (χ), Chemical softness (S) and chemical hardness (η) can be calculated according to the following formulas [22,26]:

$$\mu = \frac{E_{LUMO} + E_{HOMO}}{2}$$

$$\chi = -\mu = -\frac{E_{LUMO} + E_{HOMO}}{2}$$

$$\eta = \frac{E_{LUMO} - E_{HOMO}}{2}$$

$$S = \frac{1}{2\eta}$$

For the compounds under study, the total dipole moment (μ),[27] the average linear polarizability (α),[28] the hyperpolarizability (β),[29] and the anisotropy of polarizability (Δα), [30] were evaluated according to:

$$\mu = \sqrt{\mu_x^2 + \mu_y^2 + \mu_z^2}$$

$$\alpha = \frac{1}{3}.(\alpha_{xx} + \alpha_{yy} + \alpha_{zz})$$

$$\beta = \sqrt{\beta_x^2 + \beta_y^2 + \beta_z^2}$$

$$\Delta\alpha = \sqrt{\frac{(\alpha_{xx} - \alpha_{yy})^2 + (\alpha_{yy} - \alpha_{zz})^2 + (\alpha_{zz} - \alpha_{xx})^2}{2}}$$

2.2. Validation of the Calculation Method

All quantum chemical calculations in this study were performed using the Gaussian 09 software package. The graphical interface GaussView 6.0.16 was employed to visualize the simulated absorption spectra and analyze the molecular orbital density distributions. The hybrid exchange-correlation functional B3LYP (Becke, three-parameter, Lee-Yang-Parr),[24] in conjunction with the double-polarized Pople basis set 6-311G(d,p), was employed to optimize the ground-state geometries of all studied molecules. This level of theory was also used to compute the total reorganization energies (λ_{total}) for both anionic and cationic states, as well as to determine the energies of the frontier molecular orbitals (HOMO and LUMO) and the corresponding energy gaps.

This computational approach has proven particularly reliable for molecular systems with D-π-A architectures. [15,31] The optimized geometries were confirmed to be true minima on the potential energy surface, as indicated by the absence of imaginary vibrational frequencies.

Previous studies have also demonstrated that a variety of exchange-correlation functionals can predict the absorption spectra of organic molecules with reasonable accuracy.[25,32] However, selecting a functional that is truly well-suited for a specific class of compounds remains a challenging task. In this study, four exchange-correlation functionals, CAM-B3LYP, PBEPBE, B3PW91, and B3LYP,[33,34] were evaluated to assess their predictive accuracy regarding the absorption spectra of dye D_0.

As summarized in **Fig. 2**, CAM-B3LYP exhibited the best agreement with the experimental λ_{max} values. Consequently, the CAM-B3LYP functional, in combination with the 6-311G basis set, was selected for all TD-DFT calculations performed in this work. Closely related DFT protocols have been applied to molecules bearing similar structural segments, supporting the relevance and transferability of our methodological framework.[55,56]

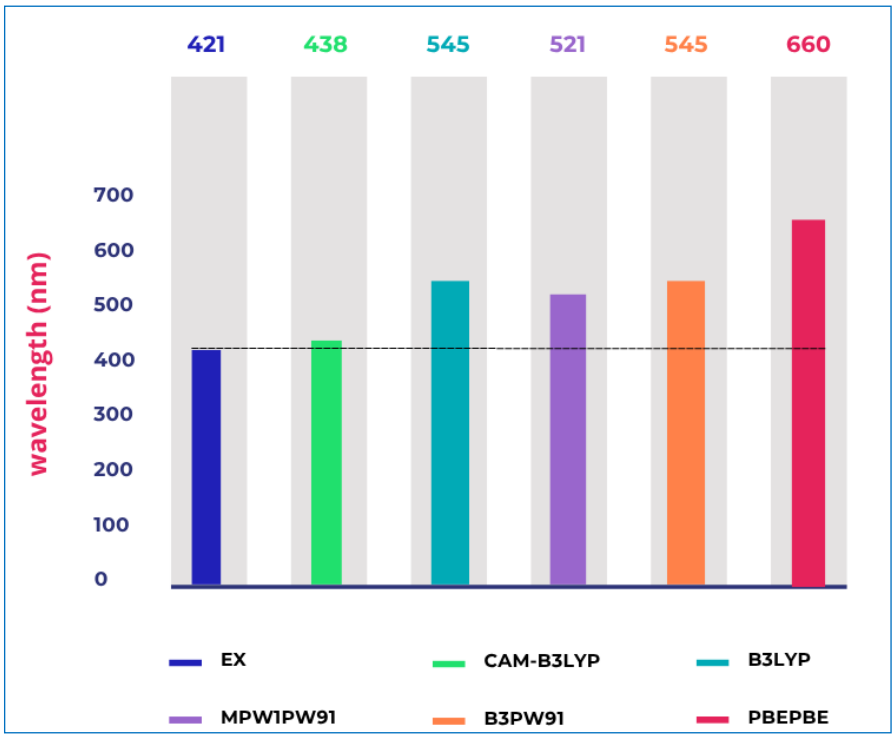

Fig. 2. Analyzing the functional employed in the TD-DFT calculation for determining the maximum absorption wavelengths (λ_{max}) for D_0.

3. Results and discussion

3.1. Synthesis and characterization of the reference dye D_0

Aldehyde 2 (0.81 mmol) was coupled with 4-ethynyl-N,N-dimethylaniline 1 (0.114 g, 0.78 mmol) in a mixture of THF (10 mL), trimethylamine (6 mL), $Pd(PPh_3)_2Cl_2$ (0.023 g, 0.02 mmol), and copper(I) iodide (0.002 g, 0.01 mmol),[11] under a nitrogen atmosphere and reflux conditions. The reaction progress was monitored by thin-layer chromatography (TLC), which indicated completion after 16 hours. Upon cooling to room temperature, 10 mL of water were added, and the mixture was extracted with dichloromethane (3 × 20 mL).[11] The combined organic phases were dried over anhydrous $MgSO_4$, filtered, and concentrated under reduced pressure. The crude product was purified by silica gel column chromatography using mixtures of chloroform and petroleum ether with increasing polarity, affording the pure compound 3.[11]

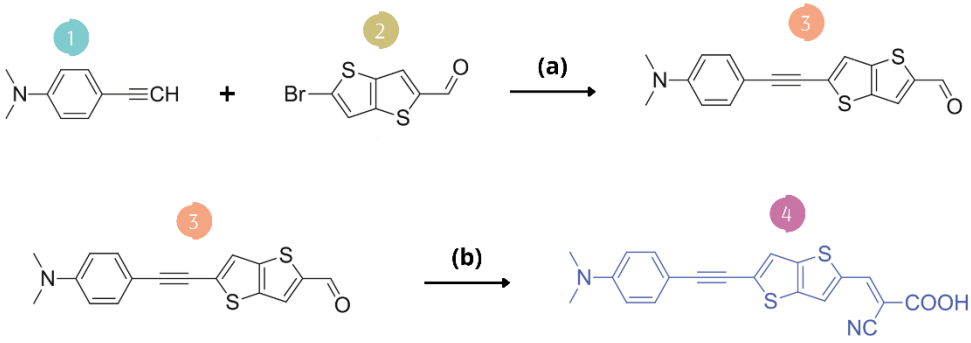

Scheme 1. Synthetic route to synthesize organic dyes D_0 and reagents:(a) THF, trimethylamine (TEA), $Pd(PPh_3)_2Cl_2$, CuI, reflux under N_2 atmosphere; (b) ethanol, cyanoacetic acid, TEA and reflux.

In a subsequent step, a mixture of aldehyde 3 (0.25 mmol) and 2-cyanoacetic acid (0.30 mmol) in ethanol (15 mL) was treated with four drops of triethylamine. The reaction mixture was refluxed for 6 hours, then cooled to room temperature. After partial evaporation of the solvent, diethyl ether was added to induce precipitation. The resulting solid was collected by filtration, washed with diethyl ether, and dried to afford the pure compound 4 **(D_0)** (**Scheme 1**).[11]

The synthesized organic dyes D_0 was fully characterized using spectroscopic and analytical techniques: UV-Vis (ethanol) λ_{max} = 421 nm ($\varepsilon = 3.4 \times 10^4$ M^{-1} cm^{-1}); ^{1}H NMR (DMSO-d_6, 400 MHz) δ 2.96 (s, 6H, NCH_3), 6.71 (d, 2H), 7.38 (d, 2H), 7.70 (s, 1H), 7.98 (s, 1H), 8.15 (s, 1H, =CH); HRMS (ESI) m/z = 379.0569 ($[M + H]^+$, calc. 379.0497).[11]

3.2. Structural properties

Organic dyes play a fundamental role as sensitizers in dye-sensitized solar cells (DSSCs), where they are responsible for absorbing sunlight and generating photoexcited electrons. A deep understanding of their structural characteristics is essential for optimizing electron injection mechanisms.[35,36] Among the different molecular components, the donor groups critically influence the absorption spectra, the HOMO-LUMO energy gap, and the intramolecular charge transfer (ICT) properties. In an effort to design efficient sensitizers, we developed a series of D-π-A organic dyes, labeled **D_1-D_{19}**, by systematically modifying the donor units of the reference dye **D_0**.

Electron-donating groups generally shorten bond lengths by increasing electron density between bonded atoms, thereby strengthening the bond. The incorporation of such donor moieties can thus significantly alter bond lengths and consequently affect the overall geometry of the molecule.[25,37]

The optimized geometric parameters of all investigated sensitizers are summarized in **Table 1**, where r denotes the calculated bond lengths between the donor unit and the π-conjugated spacer. All calculations were carried out using Density Functional Theory (DFT) with the B3LYP functional and the 6-31G basis set, a computational level widely recognized for its accuracy in predicting reliable molecular geometries, especially in the context of DSSCs.

Table. 1. Selected bond lengths (in Å) of the designed structures.

Dye	r (Å)	Dye	r (Å)	Dye	r (Å)
D_0	1.414	D_7	1.419	D_{14}	1.422
D_1	1.415	D_8	1.397	D_{15}	1.397
D_2	1.342	D_9	1.419	D_{16}	1.422
D_3	1.413	D_{10}	1.419	D_{17}	1.422
D_4	1.401	D_{11}	1.393	D_{18}	1.421
D_5	1.396	D_{12}	1.391	D_{19}	1.338
D_6	1.397	D_{13}	1.422		

The measured bond distance values (**Table 1**) confirm that the nature of the donor group incorporated into the D-π-A architecture strongly modulates the local geometry between the donor and the π-conjugated bridge. A detailed analysis reveals that eleven dyes (D_1, D_2, D_3, D_4, D_5, D_6, D_8, D_{11}, D_{12}, D_{15}, and D_{19}) display D-π bond lengths that are significantly shorter than that observed in the reference molecule D0. This reduction in bond length reflects enhanced electronic coupling between the donor and the π-bridge, which is generally associated with a more planar molecular conformation. Increased planarity facilitates orbital overlap and electron delocalization, both of which are key factors for fast and efficient intramolecular charge transfer, a crucial criterion for the photovoltaic performance of DSSCs.[5] Conversely, certain dyes such as D_{13}, D_{14}, D_{16}, D_{17}, and D_{18} exhibit markedly longer bond lengths. This phenomenon suggests less optimal orbital overlap, which may result from steric effects imposed by the size or conformation of the donor group, or from less efficient electronic conjugation. Such twisted geometries limit electron flow from the donor to the π-bridge, which can diminish the efficiency of intramolecular charge transfer and, consequently, the overall performance of the sensitizer.

These results, consistent with recent literature,[13,16,38] underscore the crucial importance of finely tuning both the electronic and steric properties of donor groups in the rational design of organic dyes for DSSCs. The judicious selection of the donor group thus enables control over local geometry, orbital overlap, and ultimately, the expected photovoltaic performance.

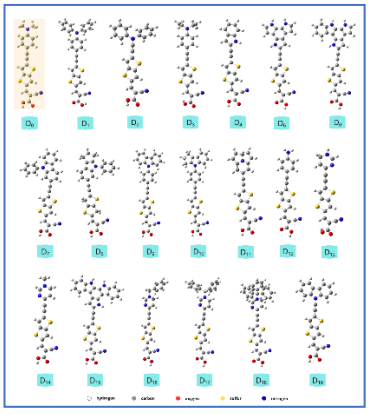

Fig. 3. Optimized ground state geometries of the dyes.

3.3. Electronic properties

Density Functional Theory (DFT) is a powerful computational tool for investigating the electronic structure of organic dyes, particularly with respect to energy levels, molecular orbitals, and charge distribution. Such insights are essential for predicting absorption spectra, charge transfer dynamics, and the overall performance of photovoltaic devices. [39,40]

Fig. 4 reports the calculated values of E_{HOMO}, E_{LUMO}, and E_{gap} for 19 dyes, determined using the B3LYP/6-311G+(d,p) level of theory. Notably, the HOMO energies of all dyes are lower than the redox potential of the I^-/I^{3-} electrolyte (-4.8 eV),[16] indicating that oxidized dyes can be efficiently regenerated through electron transfer from the electrolyte. Moreover, the LUMO levels are higher than the conduction band edge of TiO_2 (-4.0 eV), enabling efficient electron injection from the excited dye into the semiconductor.

The calculated E_{HOMO} values range from -5.3 to -5.9 eV, while E_{LUMO} values span from -3.1 to -3.5 eV. A lower HOMO energy is generally associated with improved electron-donating ability. In this context, dyes D_5, D_6, D_{15}, and D_8 exhibit notably low E_{HOMO} values, reflecting a strong potential for electron donation.

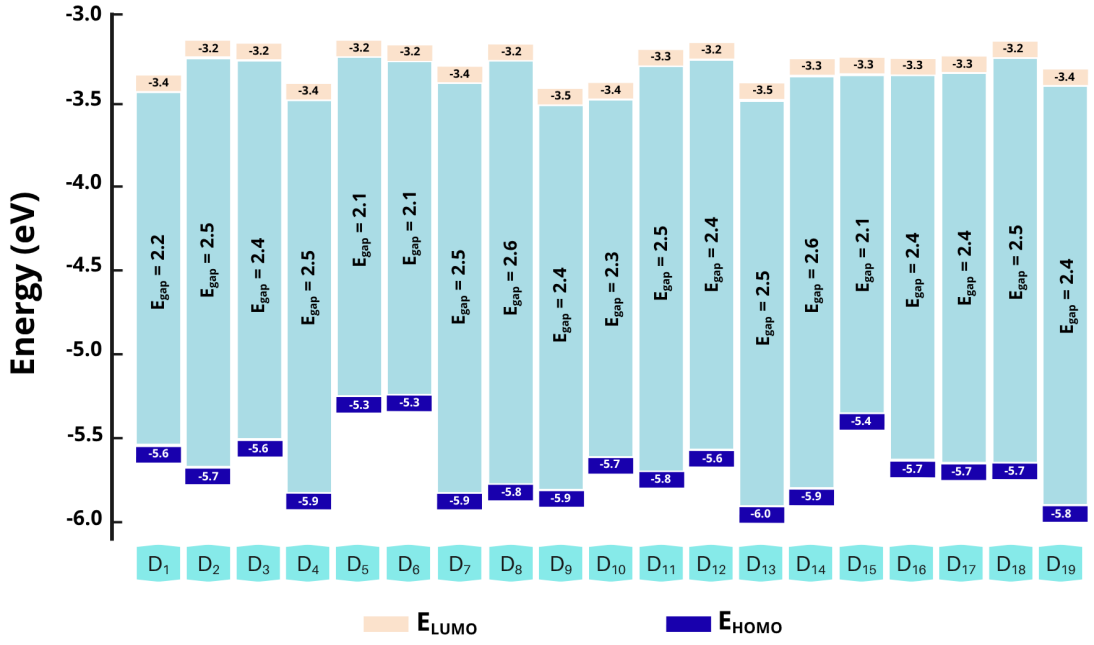

Fig. 4. Energy levels of the studied molecules obtained by B3LYP/6-311G+(d,p) computed in the gas phase.

A narrower HOMO-LUMO gap typically facilitates electronic transitions. Among the studied dyes, compounds D_6, D_{15}, D_5, D_{10}, D_1, D_3 and D_{16} show HOMO-LUMO gaps comparable to or smaller than that of the reference dye D_0 (2.4 eV),[11] indicating a reduced barrier for electronic transitions and the ability to absorb lower-energy photons.

3.4. Electronic Absorption Spectra

The absorption spectra of the investigated dyes predominantly exhibit a low-energy electronic transition associated with a strong oscillator strength, resulting in high light-harvesting efficiency (LHE) values.

Table 2 summarizes the maximum absorption wavelengths (λmax) and LHE values for all studied dyes. All compounds demonstrate absorption bands within the visible region. Notably, dyes containing donor units D_1, D_3, D_5, D_6, D_8, and D_{15} display λmax values equal to or higher than that of the reference dye D_0 (442.70 nm).

Among them, dyes with D_1, D_3, D_5, D_6, D_8 and D_{15} exhibit a distinct red-shift in absorption maxima, identifying them as promising candidates for photovoltaic applications. This red-shift trend is consistent with the calculated HOMO-LUMO gap values.

These results clearly indicate that the nature of the donor group has a substantial impact on the optical behavior of the dyes. Variations in λmax and LHE reflect enhanced electronic coupling and improved visible-light absorption, particularly for dyes incorporating **D_1, D_3, D_5, D_6, D_8 and D_{15}** donor moieties.

Additionally, the energy levels and spatial distributions of frontier molecular orbitals play a pivotal role in the observed electronic excitation processes.

Table. 2. Calculated maximum absorption wavelengths (λmax, in nm) and corresponding light-harvesting efficiency (LHE) values of the various dye sensitizers.

Donors	λmax (nm)	f	LHE	Donors	λmax (nm)	f	LHE
D_0	442.7	1.7274	0.9812	D_{10}	418.09	1.8465	0.9857
D_1	449.33	1.8412	0.9855	D_{11}	407.08	1.338	0.9540
D_2	432.53	1.3688	0.9572	D_{12}	433.38	1.6234	0.9761
D_3	440.1	1.7123	0.9806	D_{13}	406.31	1.2663	09458
D_4	428.58	1.7566	0.9824	D_{14}	406.67	1.2598	0.9450
D_5	471.99	1.8348	0.9853	D_{15}	470.76	1.8832	0.9869
D_6	476.88	1.8408	0.9855	D_{16}	409.14	1.3473	0.9550
D_7	421.98	1.8985	0.9873	D_{17}	411.3	1.3678	0.9571
D_8	444.2	1.7152	0.9807	D_{18}	409.85	1.4708	0.9661
D_9	413.59	1.8426	0.9856	D_{19}	412	1.3091	0.9509

3.5. Frontiers molecular orbitals

The spatial distribution of charge density within molecular orbitals is a key factor that influences the electronic properties and photovoltaic performance of organic dyes. In photovoltaic materials, efficient charge delocalization in the HOMO facilitates hole mobility, while appropriate localization of the LUMO, particularly over the acceptor units, enhances electron transport.[25]

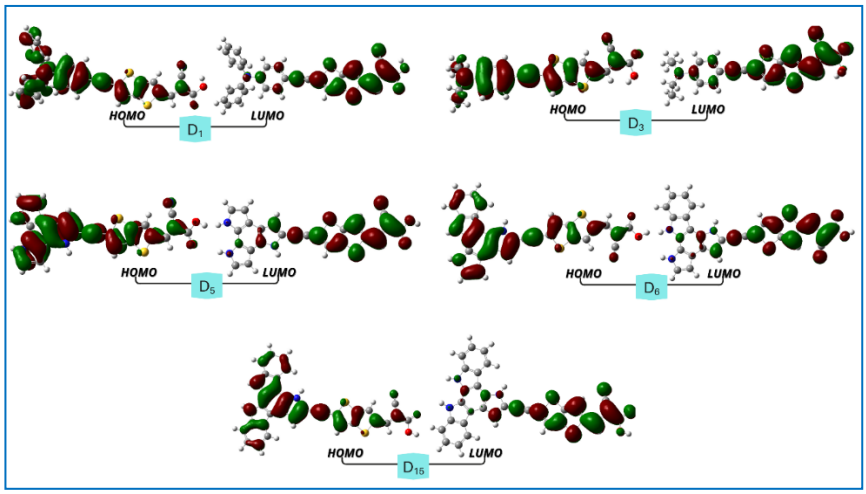

Fig. 5. The contour plots of HOMO and LUMO orbitals of the all dyes, computed in the gas phase.

The frontier molecular orbital (HOMO-LUMO) profiles of the selected dyes, along with their corresponding electronic transitions, are illustrated in **Fig. 5**. Only **the five** most promising dyes **(D_1, D_3, D_5, D_6, and D_{15})** were included in this analysis, as well as in all subsequent analyses, due to their outstanding electronic performance.

As shown in **Fig. 5**, the analysis of the five selected dyes highlights a consistent distribution of electron density across the frontier molecular orbitals. In most cases, the HOMO electron density is primarily concentrated on the donor unit, with partial delocalization extending into the π-spacer adjacent to the auxiliary acceptor. In contrast, the LUMO electron density is mainly localized over the π-conjugated bridge and the acceptor groups. This electron density distribution is characteristic of a π→π* transition, suggesting an efficient transfer of the photoexcited electrons into the conduction band of TiO_2.[41,42]

3.6. Electrostatic Potentials

The electron density is a key parameter for understanding the reactivity of nucleophilic and electrophilic sites, as well as elucidating hydrogen bonding interactions, biological recognition processes, and its correlation with various macroscopic properties for predictive purposes. [43,44]

This property is directly related to the molecular electrostatic potential (MEP). The MEP surfaces were computed using the DFT/B3LYP/6-311G(d,p) method on the optimized geometries.

Fig. 6 presents a color-coded potential map distinguishing region according to their electron density: the red-to-green range corresponds to electron-rich regions favorable for electrophilic attack via proton attraction, whereas the green-to-blue range denotes nucleophilic regions characterized by proton repulsion. Green represents a zero potential. The potential gradient providing a visual guide for interpreting molecular reactivity.

Analysis of the MEP maps reveals that positive electrostatic potentials dominate the surface of all dyes: donor units and π-bridges (comprising carbon, hydrogen, and nitrogen atoms) are mainly localized in blue regions. Conversely, red zones are predominantly concentrated around oxygen and nitrogen atoms within the acceptor units.

3.7. Density of states (DOS)

Numerous studies have demonstrated that the analysis of the Density of States (DOS) is a valuable tool for characterizing the electronic behavior of materials, particularly in the field of photovoltaics. It also enables the identification of the contributions from the molecular orbitals (MOs) of each molecular fragment to the overall electronic structure of the system.[45] DOS profiles can be generated using software such as GaussSum, which allows for a detailed decomposition based on orbital origin. **Fig. 7** presents the DOS profiles of the dyes D_1, D_3, D_5, D_6, and D_{15}, computed at the B3LYP/6-311G(d,p) level. The pronounced peaks observed in the spectra correspond to energy levels with a high density of states, directly influencing charge transfer processes in photovoltaic devices.[46,47] In these plots, the HOMO and LUMO energy levels are represented by brown and green lines, respectively, with the region between them corresponding to the band gap. These values are consistent with the E_{gap} obtained from frontier molecular orbital (FMO) analysis.

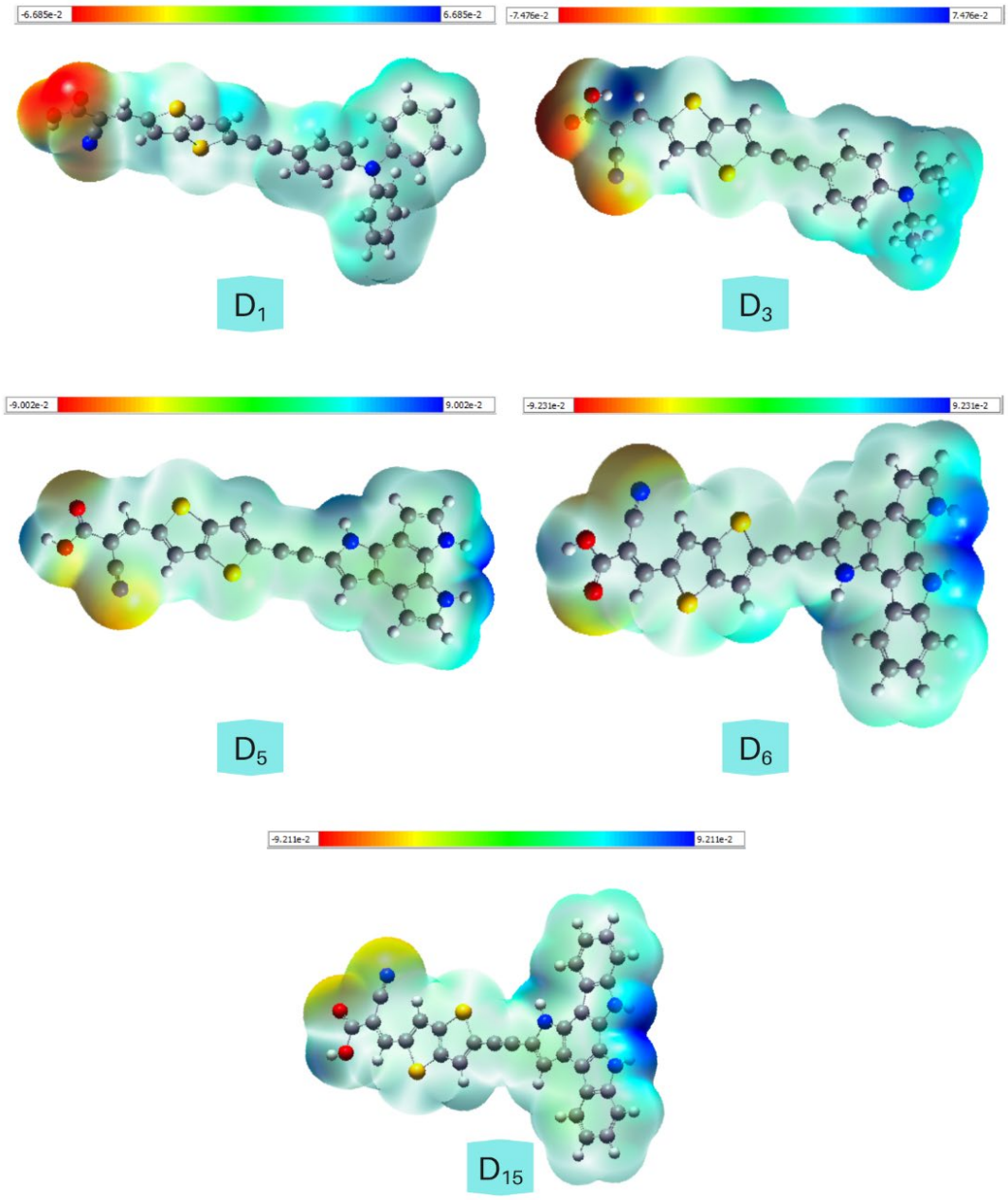

Fig. 6. Calculated electrostatic potential surfaces on the molecular surfaces of studied dyes.

Derivatives D_3, D_5, and D_6 exhibit a virtual orbital region (LUMO side) rich in closely spaced peaks, which is favorable for electron acceptance and injection into the semiconductor. D_5 and D_6 also display a broadened occupied orbital region (HOMO side), indicative of improved electronic delocalization and optimized charge transport. D_{15} shows a balanced profile, with a dense and finely structured virtual orbital region, providing a good compromise between transfer efficiency and stability. These variations in the DOS, driven by the nature of the donor units, confirm their key role in optimizing DSSC performance.

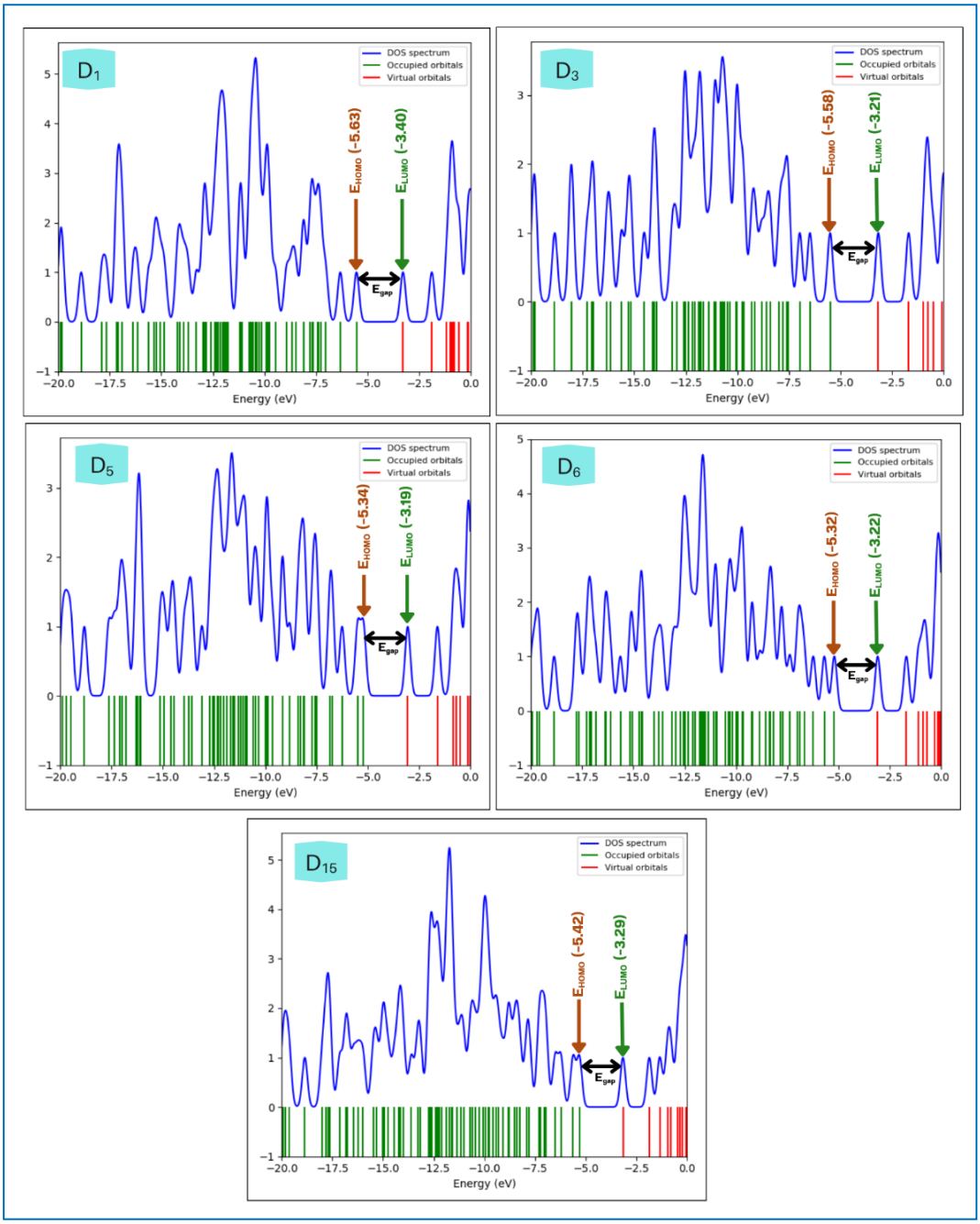

Fig. 7. Density of states and energy levels (in eV) of the examined molecules by B3LYP/6-311G (d, p). computed in the gas phase.

3.8. Chemical concepts of reactivity

As shown in **Table 3**, TiO_2 exhibits the lowest chemical potential (-4.6 eV)[48] compared to the selected dyes (D_1, D_3, D_5, D_6, and D_{15}). This difference indicates that electron transfer from the dyes, acting as electron donors, to TiO_2, serving as the electron acceptor, is both thermodynamically favorable and likely to occur spontaneously. Moreover, the chemical hardness (η) values of all dyes are lower than that of TiO_2 (η = 3.78 eV), suggesting a higher propensity of these molecules to donate one or more electrons to the semiconductor. Additionally, the electronegativity of TiO_2 (4.66 eV), which exceeds that of the dyes, further confirms its strong ability to attract and accept electrons from these donor molecules. Comparative analysis

shows that dyes D_1, D_3, D_5, D_6, and D_{15} display slightly lower chemical hardness ($\eta \approx 1.1$ eV) and higher softness ($S \approx 0.5$ eV^{-1}) than the reference dye D_0 ($\eta = 1.2$ eV, $S = 0.4$ eV^{-1}). These shifts are consistent with greater polarizability a nd an enhanced capacity to reorganize electron density upon excitation, thereby facilitating intramolecular charge transfer (ICT). A modest increase in electronegativity ($\chi \approx 4.4 – 4.5$ eV) for these systems points to a balanced electronic distribution, which supports efficient electron injection into the TiO_2 conduction band.

Table 3. Chemical potential (μ), chemical hardness (η), softness (S), and electronegativity (χ) for TiO_2 and the selected dyes, computed in the gas phase.

dye	E_{HOMO}	E_{LUMO}	μ (ev)	Ƞ (ev)	S (ev^{-1})	χ (ev)
D_0	-5.5	-3.2	-4.4	1.2	0.4	4.4
D_1	-5.6	-3.4	-4.5	1.1	0.4	4.5
D_3	-5.6	-3.2	-4.4	1.2	0.4	4.4
D_5	-5.3	-3.2	-4.3	1.1	0.5	4.3
D_6	-5.3	-3.2	-4.3	1.1	0.5	4.3
D_{15}	-5.4	-3.3	-4.4	1.1	0.5	4.4
TiO_2 [48]	-	-4.0	−4.6	3.8	0.1	4.6

3.9. Optical properties

The photovoltaic performance of dye-sensitized systems is strongly dependent on the ability of the dyes to efficiently harvest photons. An ideal photovoltaic material should exhibit broad and intense absorption across the entire visible spectrum to ensure maximum energy capture and conversion.[49,50] In this work, the impact of donor group modification on the optical properties of the proposed dyes (D_1, D_3, D_5, D_6, and D_{15}), derived from the reference dye D_0, was investigated to gain deeper insight into their potential electronic transitions. The calculations were performed using time-dependent density functional theory (TD-DFT) with the CAM-B3LYP functional and the 6-311G basis set.[48,51] The simulated absorption spectra of the reference dye D_0 and its derivatives (D_1, D_3, D_5, D_6, and D_{15}) are shown in **Fig. 8**, with the corresponding values summarized in **Table 4**. The results indicate that all five compounds display intense absorption within the UV-Vis range, spanning from 449,35 nm to 476,88 nm, corresponding to a transition from the ground state (S_0) to the first excited state (S_1). The strong agreement between theoretical predictions and available experimental data,[11] confirms the reliability of the employed methodology. The absorption profiles are dominated by a low-energy transition (≈ 2.6 eV) associated with high oscillator strengths (≈ 1.9), indicating efficient light-harvesting capability in the visible region. The most intense absorption bands primarily originate from the HOMO → LUMO transition, while the HOMO-1 → LUMO and HOMO-2 → LUMO transitions are frequently observed as secondary promotions. Overall, the modification of donor groups significantly enhances the light-harvesting efficiency of D-π-A type dyes and contributes to the optimization of their photovoltaic performance.[42]

Table. 4. The calculated values of optical parameters for PCC derivatives calculated by the CAM-B3LYP /6-311G method, computed in the gas phase.

Compound	E_{ex} (eV)	λ (nm)	f	Major contribution
D_1	2.8	449	1.841	H → L (75%) H-1→L (21%)
	3.7	336	0.021	H-1→ *L* (70%) H→L (15%)
	3.9	347	0.060	H-2 →L (100%)
D_3	2.8	450	1.712	H → L (86%) H-1→L (1%)
	3.9	319	0.015	H-1→ *L* (72%) H-2 →L (17%) H → L (10%)
	4.0	312	0.075	H-2 →L (91%) H-1→L (9%)
D_5	2.6	473	1.835	H → L (84%) H-2 →L (9%)
	3.4	363	0.036	H-1→ *L* (88%)
	3.8	323	0.038	H-2 →L (78%) H-3 →L (10%)
D_6	2.6	477	1.841	H → L (83%) H-2 →L (11%)
	3.5	353	0.097	H-1 →L (75%) H-2 →L (11%)
	3.7	331	0.024	H-2 →L (67%) H-1 →L (13%)
D_{15}	2.6	471	1.883	H → L (84%) H-2 →L (12%)
	3.4	366	0.056	H-1 →L (88%) H-1 →L+1 (12%)
	3.7	336	0.054	H-2 →L (65%) H-3 →L (10%)

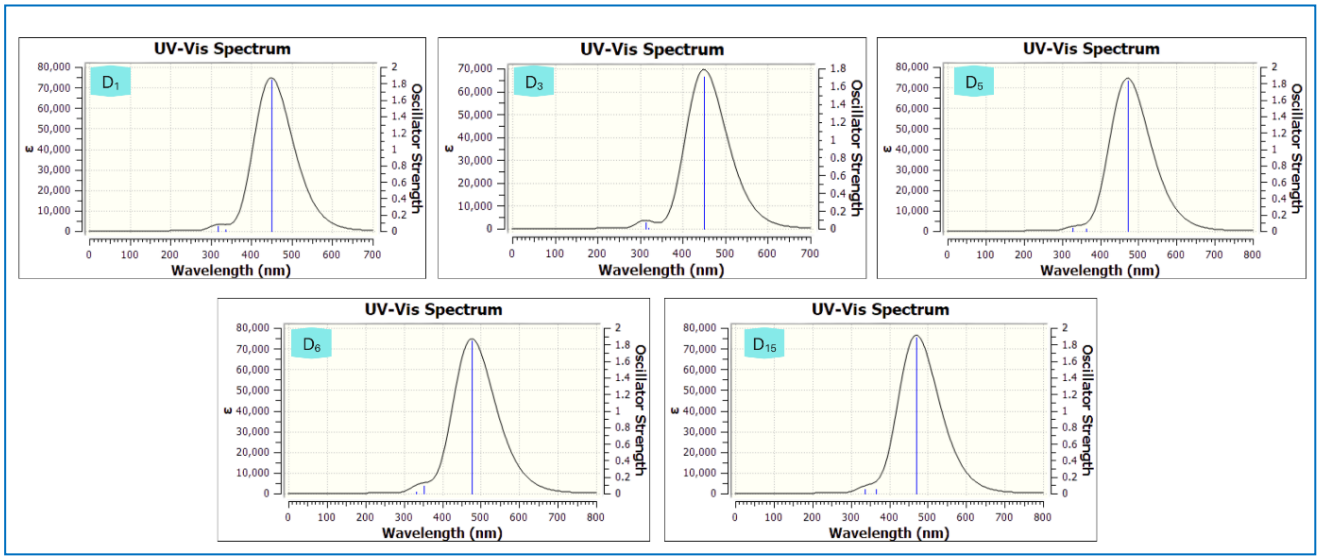

Fig. 8. Absorption spectra of the studied dyes

3.10. Photovoltaic properties

Table 5 presents the photovoltaic parameters derived from the established equations. All dyes (D_1, D_3, D_5, D_6, and D_{15}) possess excited-state energies (E_{ex}) located above the conduction band (CB) of TiO_2. The negative ΔG_{inj} values recorded for each dye confirm a spontaneous and thermodynamically favorable electron transfer from the excited state to the TiO_2 CB. In particular, D_5 and D_6 exhibit the largest negative ΔG_{inj} amplitudes, indicating an enhanced electron injection capability.

For efficient charge regeneration, minimizing ΔG_{reg} is essential. As shown in Table 5, all derivatives, except D_1, have ΔG_{reg} values comparable to or lower than that of the reference molecule D_0 (0.7 eV), thereby ensuring a sufficient driving force to achieve high power conversion efficiency (PCE) in DSSCs. The lowest ΔG_{reg} value (0.4 eV), obtained for D_5 and D_6, highlights their optimal performance.

The open-circuit voltages (V_{oc}) of these dyes range from 0.55 to 0.81 V, with a maximum variation of 0.26 V between compounds, a difference unlikely to substantially influence overall device efficiency.

Table. 5. Calculated electronic properties of the studied dyes (in eV).

dye	E^{dye}	E_{ex}	E^{dye*}	ΔG_{injec}	ΔG_{reg}	V_{oc}
D_0	5.6	2.8	2.8	-1.3	0.7	0.8
D_1	5.6	2.8	2.9	-1.1	0.8	0.6
D_3	5.6	2.7	2.8	-1.2	0.8	0.5
D_5	5.3	2.6	2.7	-1.3	0.5	0.8
D_6	5.3	2.6	2.7	-1.3	0.5	0.8
D_{15}	5.4	2.6	2.8	-1.2	0.6	0.7

3.11. Nonlinear optical properties (NLO)

The mean polarizability (α) and the first-order hyperpolarizability (β) are the principal descriptors of the nonlinear optical (NLO) response of organic dyes. Push-pull D-π-A typically display promising NLO activity,[52] because they promote π-electron delocalization and intramolecular charge transfer (ICT), two features closely associated with efficient injection of the photoexcited dye into the TiO_2 conduction band.[53] Consequently, maximizing α and β is a central design objective for new D-π-A chromophores.[54] For the selected dyes, α, β, and the polarizability anisotropy (Δα) were computed at the CAM-B3LYP/6-31G(d,p) level; numerical values are reported in **Table 6**. The descending order of α is: $D_{15} > D_6 > D_1 > D_5 > D_3 > D_0$, while the descending order of β is: $D_6 > D_5 > D_{15} > D_1 > D_3 > D_0$. Relative to the reference dye D_0, all derivatives exhibit larger β and α values, indicating an enhanced propensity for ICT and, by extension, the potential for a stronger photocurrent response. Dyes D_6, D_5, and D_{15} combine higher α, larger β, and increased dipole moments, pointing to reinforced intramolecular charge transfer. This profile positions them as promising candidates for advanced nonlinear-optical materials and as efficient sensitizers in dye-sensitized solar cells.

Table 6. Computed polarizability α , hyperpolarizability β.

dye	μ (Debye)	$\Delta\alpha.10^{-24}$ esu	$\alpha. 10^{-24}$ esu	$\beta. 10^{-30}$ esu
D_0	**11.628**	**105.510**	**60.980**	**348.980**
D_1	10.642	112.380	78.68	412.500
D_3	14.366	107.780	65.030	390.000
D_5	11.540	128.270	74.660	549.540
D_6	10.69	131.590	82.95	579.98
D_{15}	10.120	132.789	90.765	546.216

4. Conclusion

In summary, this study aims to identify optimal donor motifs for the novel organic dye D_0 (2-cyano-3-[2′-(2″-(4″-(dimethylamino)phenyl)ethynyl)thieno[3,2-b]thiophen-5′-yl]acrylic acid) and to quantify how donor substitution governs geometry, charge-transfer behavior, spectral properties and nonlinear-optical (NLO) responses. To this end, we performed density-functional theory (DFT) and time-dependent DFT (TD-DFT) calculations.

The donor units D_5, D_6, and D_{15} exhibit efficiencies markedly higher than those of previously reported sensitizers. This enhancement is attributed to the presence of multiple conjugated nitrogen atoms, benzenoid rings, and indole cores, which collectively strengthen electron donation and π-delocalization.The selected dyes D_5, D_6, and D_{15} emerge as the most promising candidates, combining a lower HOMO level, a narrower E_{gap} enhanced absorption intensity, and a pronounced bathochromic shift of the main absorption band.

The selected dyes also exhibit negative electron-injection free energies (ΔG_{inj}), consistent with spontaneous electron transfer from the excited dye to the TiO_2 conduction band. Notably, D5 and D6 display the lowest regeneration free energies (ΔG_{reg}), indicating particularly efficient dye regeneration and elevated open-circuit voltages (V_{oc}).In parallel, D_5, D_6, and D_{15} exhibit high polarizabilities (α) and first-order hyperpolarizabilities (β), indicating efficient sensitization under photoexcitation and strong potential for nonlinear-optical (NLO) applications.

Taken together, these findings validate a rational molecular-engineering strategy for D-π-A chromophores and identify the designed dyes as strong sensitizer candidates for dye-sensitized solar cells (DSSCs).

References

1. Ramasamy S., Bhagavathiachari M., Suthanthiraraj S. A., and Pichai M. **(2022)** Mini review on the molecular engineering of photosensitizer: current status and prospects of metal-free/porphyrin frameworks at the interface of dye-sensitized solar cells. *Dyes Pigments*, 203, 110380.
2. Boutkbout Nait Moudou M., EL Ouafy H., Halil L., Aamor M., Naciri S., Chriyaa M.R., Iken W., and EL Ouafy T. **(2025)** Computational DFT study on donor and spacer substitution in arylamine-based push-pull molecules for enhanced photovoltaic performance. *Phys. Chem. Res.*, 13 (2).
3. Halil L., EL Ouafy H., Boutkbout Nait Moudou M., Aamor M., Chriyaa M. R., Iken W., Naciri S., and EL Ouafy T. **(2025)** Study of the synthesis reactivity of flavonol derivatives using quantum calculation methods. *Chem. Rev. Lett.*, 8 (2)
4. Hagfeldt A., Boschloo G., Sun L., Kloo L., and Pettersson H. **(2010)** Dye-sensitized solar cells. *Chem. Rev.*, 110 (11), 6595–6663.
5. Yang J., Ganesan P., Teuscher J., Moehl T., Kim Y. J., Yi C., Comte P., Pei K., Holcombe T. W., Nazeeruddin M. K., Hua J., Zakeeruddin S. M., Tian H., and Grätzel M. **(2014)** Influence of the donor size in D–π–A organic dyes for dye-sensitized solar cells. *J. Am. Chem. Soc.*, 136 (15), 5722–5730.
6. Sen A., Putra M. H., Biswas A. K., Behera A. K., and Groβ A. **(2023)** Insight on the choice of sensitizers/dyes for dye sensitized solar cells: a review. *Dyes Pigments*, 213, 111087.
7. Iken W., EL Ouafy H., Halil L., Naciri S., Boutkbout Nait Moudou M., Aamor M., Chriyaa M. R., and EL Ouafy T. **(2025)** Effect of gold slab layers relaxation on adsorption of alkanethiols on the (111) surface: a density functional theory study. *J. Mol. Model.*, 31 (7), 182.
8. Iswarya S., Dharshini A., Scholastica Mary Vithiya B., and Augustine Arul Prasad T. **(2025)** Evolving smart homes to exploring space, dye-sensitized solar cells (DSSC) as a sustainable energy model for the future world—a review. *Energy*, 8, 100328.
9. Chriyaa M. R., El Ouafy H., Iken W., Naciri S., Boutkbout Nait Moudou M., Aamor M., Halil L., and El Ouafy T. **(2025)** Exploring the impact of spacers in novel indole-based D–π–D–A dyes for high-efficiency DSSCs: a DFT/TD-DFT study. *Curr. Chem. Lett.*, 14 (3), 533–546.
10. Hagberg D. P., Edvinsson T., Marinado T., Boschloo G., Hagfeldt A., and Sun L. **(2006)** A novel organic chromophore for dye-sensitized nanostructured solar cells. *Chem. Commun.*, (21), 2245.
11. Fernandes S. S. M., Mesquita I., Andrade L., Mendes A., Justino L. L. G., Burrows H. D., and Raposo M. M. M. **(2017)** Synthesis and characterization of push-pull bithiophene and thieno[3,2-b]thiophene derivatives bearing an ethyne linker as sensitizers for dye-sensitized solar cells. Org. Electron., 49, 194–205.
12. Sahu P. N., Vasarla A. D., Kumili R. K., and Sen A. **(2024)** Optimal donor groups for novel organic dye "3-(5-(4-(diphenylamino)styryl)thiophen-2-yl)-2-cyanoacrylic acid" in the context of N-type dye-sensitized solar cells: a theoretical investigation. *Comput. Theor. Chem.*, 1241, 114901.
13. Fadili D., Fahim Z. M. E., Alioui A., Bouzzine S. M., and Hamidi M. **(2024)** Enhancing optoelectronic properties of phosphonic acid based dyes via donor unit variation: a DFT/TD-DFT investigation. *Mater. Today Commun.*, 38, 108126.
14. Ran X., Zhao C., Yin M., Li K., Yu X., and Jin L. **(2025)** Design and screening on D-A-π-A type sensitizers for dye-sensitized solar cells: effects of various donors on photovoltaic performances. *Comput. Theor. Chem.*, 1245, 115101.

15. Roohi H., and Mohtamadifar N. **(2022)** The role of the donor group and electron-accepting substitutions inserted in π-linkers in tuning the optoelectronic properties of D–π–A dye-sensitized solar cells: a DFT/TDDFT study. *RSC Adv.*, 12 (18), 11557–11573.
16. Nassar M. F., Abdulmalek E., Ismail M. F., and Ahmad S. A. A. **(2024)** Enhancing the performance of pyridyl carboxamide-N,N-dimethyl amino chalcone (PCC) as a dye sensitizer for dye-sensitized solar cells (DSSCs) through the incorporation of electron donor moieties. *Int. J. Electrochem. Sci.*, 19 (9), 100715.
17. Behera A. K., Sahu P. N., Shukla R., and Sen A. **(2024)** Donor effect on the B ← N dative bond directed dye sensitized solar cell application. *Comput. Theor. Chem.*, 1236, 114606.
18. Arslan B. S. **(2024)** Effect of electron donor groups on the performance of benzothiadiazole dyes with simple structures for dye-sensitized solar cells. *J. Photochem. Photobiol. Chem.*, 449, 115392.
19. Lo C.-Y., Kumar D., Chou S.-H., Chen C.-H., Tsai C.-H., Liu S.-H., Chou P.-T., and Wong K.-T. **(2016)** Highly twisted dianchoring D–π–A sensitizers for efficient dye-sensitized solar cells. *ACS Appl. Mater. Interfaces*, 8 (41), 27832–27842
20. Aamor M., EL Ouafy H., Halil L., Boutkbout Nait Moudou M., Chriyaa M. R., Iken W., Naciri S., and EL Ouafy T. **(2024)** Spectroscopic analysis and theoretical comparison of the reactivity of 6-amino-3(R)benzophenone reactions with acetylacetone. *Chem. Rev. Lett.*, 7 (10).
21. Preat J., Michaux C., Jacquemin D., and Perpète E. A. **(2009)** Enhanced efficiency of organic dye-sensitized solar cells: triphenylamine derivatives. *J. Phys. Chem. C*, 113 (38), 16821–16833.
22. Singh M., and Kanaparthi R. K. **(2022)** Theoretical exploration of 1,3-indanedione as electron acceptor-cum-anchoring group for designing sensitizers towards DSSC applications. *Sol. Energy*, 237, 456–469.
23. Liu D.-S., Ding W.-L., Zhu K.-L., Geng Z.-Y., Wang D.-M., and Zhao X.-L. **(2014)** The master factors influencing the efficiency of D–A–π–A configurated organic sensitizers in dye-sensitized solar cell via theoretically characterization: design and verification. *Dyes Pigments*, 105, 192–201.
24. Vaissier V., Barnes P., Kirkpatrick J., and Nelson J. **(2013)** Influence of polar medium on the reorganization energy of charge transfer between dyes in a dye sensitized film. *Phys. Chem. Chem. Phys.*, 15 (13), 4804.
25. Boutkbout Nait Moudou M., EL Ouafy H., Halil L., Aamor M., Naciri S., Chriyaa M. R., Iken W., and EL Ouafy T. **(2025)** Exploring the role of π-spacers in six novel push-pull photovoltaic systems based on N-methylarylamine: a theoretical DFT investigation. *Comput. Theor. Chem.*, 1244, 115023.
26. Iken W., EL Ouafy H., Aamor M., Halil L., Boutkbout Nait Moudou M., Naciri S., Chriyaa M. R., and EL Ouafy T. **(2025)** Theoretical study of 2D cancer drug nanocarriers based on calcium chloride. *J. Mol. Model.*, 31 (5), 147.
27. Muhammad S., Xu H., Su Z., Fukuda K., Kishi R., Shigeta Y., and Nakano M. **(2013)** A new type of organic–inorganic hybrid NLO-phore with large off-diagonal first hyperpolarizability tensors: a two-dimensional approach. *Dalton Trans.*, 42 (42), 15053.
28. Atalay Y., Avcı D., and Başoğlu A. **(2008)** Linear and non-linear optical properties of some donor–acceptor oxadiazoles by ab initio Hartree-Fock calculations. *Struct. Chem.*, 19 (2), 239–246.
29. Muhammad S., Al-Sehemi A. G., Su Z., Xu H., Irfan A., and Chaudhry A. R. **(2017)** First principles study for the key electronic, optical and nonlinear optical properties of novel donor-acceptor chalcones. *J. Mol. Graph. Model.*, 72, 58–69.
30. Lee M.-J., Balanay M. P., and Kim D. H. **(2012)** Molecular design of distorted push–pull porphyrins for dye-sensitized solar cells. *Theor. Chem. Acc.*, 131 (9), 1269.
31. Raftani M., Abram T., Azaid A., Kacimi R., Bennani M. N., and Bouachrine M. **(2021)** Theoretical design of new organic compounds based on diketopyrrolopyrrole and phenyl for organic bulk heterojunction solar cell applications: DFT and TD-DFT study. *Mater. Today Proc.*, 45, 7334–7343.
32. Casanova D., Rotzinger F. P., and Grätzel M. **(2010)** Computational study of promising organic dyes for high-performance sensitized solar cells. *J. Chem. Theory Comput.*, 6 (4), 1219–1227.
33. Khalid A., Khera R. A., Saeed A., Khalid M., Iqbal S., and Iqbal J. **(2021)** Designing benzothiadiazole based non-fullerene acceptors with high open circuit voltage and higher LUMO level to increase the efficiency of organic solar cells. *Optik*, 228, 166138.
34. Abubakari I. **(2025)** The 9H-carbazole based derivative dyes for dye-sensitized solar cells technology. *Comput. Theor. Chem.*, 1248, 115165.
35. Dulo B., Phan K., Githaiga J., Raes K., and De Meester S. **(2021)** Natural quinone dyes: a review on structure, extraction techniques, analysis and application potential. *Waste Biomass Valorization*, 12 (12), 6339–6374.
36. Luan F., Xu X., Liu H., and Cordeiro M. N. D. S. **(2013)** Review of quantitative structure-activity/property relationship studies of dyes: recent advances and perspectives. *Color. Technol.*, 129 (3), 173–186.
37. Investigating a boron nitride plate for the formaldehyde adsorption: density functional theory calculations. **(2022)** *Biointerface Res. Appl. Chem.*, 13 (4), 346.
38. Liu B., Zhu W., Zhang Q., Wu W., Xu M., Ning Z., Xie Y., and Tian H. **(2009)** Conveniently synthesized isophorone dyes for high efficiency dye-sensitized solar cells: tuning photovoltaic performance by structural modification of donor group in donor–π–acceptor system. *Chem. Commun.*, (13), 1766.
39. Kannan P., P S., G V., Pm A., P V., Y S. M., S K., and Erkan S. **(2021)** Synthesis, photophysical, electrochemical, and DFT examinations of two new organic dye molecules based on phenothiazine and dibenzofuran. *In Review*, December 3.

40. Periyasamy K., Sakthivel P., Vennila P., Anbarasan P. M., Venkatesh G., and Sheena Mary Y. **(2021)** Novel D-π-A phenothiazine and dibenzofuran organic dyes with simple structures for efficient dye-sensitized solar cells. *J. Photochem. Photobiol. Chem.*, 413, 113269.
41. Zhang Z.-L., Zou L.-Y., Ren A.-M., Liu Y.-F., Feng J.-K., and Sun C.-C. **(2013)** Theoretical studies on the electronic structures and optical properties of star-shaped triazatruxene/heterofluorene co-polymers. *Dyes Pigments*, 96 (2), 349–363.
42. Souilah M., Hachi M., Fitri A., Benjelloun A. T., El Khattabi S., Benzakour M., Mcharfi M., and Zgou H. **(2021)** Coumarin-based D–π–A dyes for efficient DSSCs: DFT and TD-DFT study of the π-spacers influence on photovoltaic properties. *Res. Chem. Intermed.*, 47 (2), 875–893.
43. Luque F. J., López J. M., and Orozco M. **(2000)** Perspective on "Electrostatic interactions of a solute with a continuum. A direct utilization of ab initio molecular potentials for the prevision of solvent effects." *Theor. Chem. Acc.*, 103 (3–4), 343–345.
44. Kolev T. M., Yancheva D. Y., Stamboliyska B. A., Dimitrov M. D., and Wortmann R. **(2008)** Nonlinear optical properties of pyridinium-betaines of squaric acid: experimental and theoretical study. *Chem. Phys.*, 348 (1–3), 45–52.
45. Stankevych A., Vakhnin A., Andrienko D., Paterson L., Genoe J., Fishchuk I., Bässler H., Köhler A., and Kadashchuk A. **(2021)** Density of states of OLED host materials from thermally stimulated luminescence. *Phys. Rev. Appl.*, 15 (4), 044050.
46. Shakil J. A., Saikat S. P., Bhattacharjee N., Hossain Md. R., Hossen M., Islam J., Khandaker M. U., Uddin J., and Chowdhury F. I. **(2024)** DFT/TD-DFT study of novel triphenylamine-based dyes with azo moieties and π-spacer variations for enhanced dye-sensitized solar cell performance. *Chem. Phys. Impact*, 9, 100725.
47. Saeed M. U., Iqbal J., Mehmood R. F., Akram S. J., El-Badry Y. A., Noor S., and Khera R. A. **(2022)** End-capped modification of Y-shaped dithienothiophen[3,2-b]-pyrrolobenzothiadiazole (TPBT) based non-fullerene acceptors for high performance organic solar cells by using DFT approach. *Surf. Interfaces*, 30, 101875.
48. Zhou Z., and Parr R. G. **(1989)** New measures of aromaticity: absolute hardness and relative hardness. *J. Am. Chem. Soc.*, 111 (19), 7371–7379.
49. Wong K. M., Khan W., Shoaib M., Shah U., Khan S. H., and Murtaza G. **(2018)** *Ab initio* investigation of the structural, electronic and optical properties of the $Li_2In_2XY_6$ (X = Si, Ge; Y = S, Se) compounds. *J. Electron. Mater.*, 47 (1), 566–576.
50. Ding W.-L., Wang D.-M., Geng Z.-Y., Zhao X.-L., and Xu W.-B. **(2013)** Density functional theory characterization and verification of high-performance indoline dyes with D–A–π–A architecture for dye-sensitized solar cells. *Dyes Pigments*, 98 (1), 125–135.
51. Azaid A., Raftani M., Alaqarbeh M., Kacimi R., Abram T., Khaddam Y., Nebbach D., Sbai A., Lakhlifi T., and Bouachrine M. **(2022)** New organic dye-sensitized solar cells based on the D–A–π–A structure for efficient DSSCs: DFT/TD-DFT investigations. *RSC Adv.*, 12 (47), 30626–30638.
52. Ayare N. N., Sharma S., Sonigara K. K., Prasad J., Soni S. S., and Sekar N. **(2020)** Synthesis and computational study of coumarin thiophene-based D-π-A azo bridge colorants for DSSC and NLOphoric application. *J. Photochem. Photobiol. Chem.*, 394, 112466.
53. Senge M. O., Fazekas M., Notaras E. G. A., Blau W. J., Zawadzka M., Locos O. B., and Ni Mhuircheartaigh E. M. **(2007)** Nonlinear optical properties of porphyrins. *Adv. Mater.*, 19 (19), 2737–2774.
54. Balanay M. P., and Kim D. H. **(2011)** Optical properties of porphyrin analogues for solar cells: an NLO approach. Curr. Appl. Phys., 11 (1), 109–116.
55. Łapczuk-Krygier A., Baranowska K., Ponikiewski Ł., Matern E., and Pikies J. **(2012)** π-Indenyl substituted zirconium compounds containing terminal bonded phosphanylphosphido ligands [$Ind_2Zr(Cl)\{(SiMe_3)P–P\ R_2$-κP^1}]. *Inorg. Chim. Acta*, **387** (361–365).
56. Fryźlewicz A., Olszewska A., Zawadzińska K., Woliński P., Kula K., Kącka-Zych A., Łapczuk-Krygier A. & Jasiński R. **(2022)** On the mechanism of the synthesis of nitro-functionalised Δ²-pyrazolines via [3+2] cycloaddition reactions between α-EWG-activated nitroethenes and nitrylimine TAC systems. *Organics*, 3(1), 59-76.